RSC Advances

ROYAL SOCIETY OF CHEMISTRY

www.rsc.org/advances

Cite this: DOI: 10.1039/c0xx00000x

www.rsc.org/xxxxxx

ARTICLE TYPE

Switchable fluorescent AIE-active nanoporous fibers for cyclic oil adsorption

Wei Yuan,[a] Pei-Yang Gu,[b] Cai-Jian Lu,[b] Ke-Qin Zhang,*[a] Qing-Feng Xu*[b] and Jian-Mei Lu*[b]

Received (in XXX, XXX) Xth XXXXXXXXX 20XX, Accepted Xth XXXXXXXXX 20XX

DOI: 10.1039/b000000x

Porous fibers are capable of large amounts of oil adsorption, owing to their extremely large surface area. The novel aggregation-induced-emission (AIE) -active polymer was synthesized by anchoring AIE-active initiators to the end of polymer chains through atom transfer radical polymerization. The porous fibers based on the synthesized AIE-active PMMA were fabricated through the electrospinning technique. The obtained porous fiber shows exceptional fluorescence; green fluorescence in the porous fiber can be switched off and on by the adsorption and desorption of silicon or bean oil. The fluorescence quenching phenomenon is due to the aggregation state change of the AIE molecules accompanying polymer swelling during the cyclic oil adsorption. Such fluoresent porous fibers can be used to lighten and sense the process of oil adsorption, which could have the promising applications in area of self-cleaning materials, ultra-high sensitive sensors and biomaterials.

Introduction

Although the use of conventional polymeric nanofibers is popular today, multi-functional polymeric nanofibers have attracted significant attention due to their exceptional traits and abilities. These functional nanofibers can be prepared by electrospinning[1-2] polymers blended with additional compounds such as organic/inorganic nanoparticles,[3-4] nanowires,[5-6] and proteins.[7-8] Among the various types of multi-functional nanofibers, researchers have devoted particular attention to fluorescent nanofibers, speculating promising potential in many areas due to their intriguing properties.[9-14] Although these nanofibers show advantageous characteristics, current common preparation methods are unfavourable for preparation of high-quality fluorescent nanofibers. Fluorescent nanofibers are typically prepared by electrospinning the polymer, which is doped with small fluorescent molecules[15-16] or fluorescent quantum dots.[17-18] The electrospinning process causes the small fluorescent molecules and polymers to physically mix, but an absence of chemical bonds results in vulnerability to external perturbation. The inorganic fluorescent quantum dots tend to aggregate in the polymer blend solution due to their large surface energy, making it difficult to prepare uniform fluorescent nanofibers with an even arrangement of quantum dots.[19-20] The impracticality of this preparation method necessitated the development of more feasible methods to prepare fluorescent nanofibers. This study presents a novel method to prepare fluorescent nanofibers with a basis on aggregation induced emission (AIE) mechanisms.[21-22]

In our previous studies,[23] AIE-active polymers were synthesized by anchoring AIE-active initiators to the end of polymer chains through atom transfer radical polymerization (ATRP). Commonly used polymers are Polystyrene (PS), Polymethyl Methacrylate (PMMA) and poly(2-hydroxyethyl methacrylate) (PHEMA). The fluorescence of the AIE-active polymers quenched when they were dissolved in organic solvent solution, but recovered as the polymers aggregated. The obtained AIE-active polymers are a viable candidate to use in the preparation of fluorescent fibers via electrospinning. Literature reports that during the process of electrospinning,[24-25] the high voltage-induced fluid jet forming between the electrodes is thermodynamically unstable due to solvent evaporation and moisture in surrounding environment. Porous fibers can generally be induced by the phase separation because the volatile solvent evaporates rapidly. In this study, electrospinning was utilized to fabricate novel fluorescent porous fiber via phase separation from AIE-active polymers.

Studies of porous fibers used for oil adsorption have revealed that use of porous structures enhances the capacity of oil adsorption.[26-27] However, the mechanism of oil adsorption and desorption in porous fibers is unclear. Tracing the fluorescence of AIE-active polymers in fluorescent porous fibers is a feasible model to uncover the process of oil adsorption-desorption in porous fibers. Changes in the fluorescence of porous fibers may provide meaningful indications on the interface of oil and AIE-polymers, which can be used to reveal the mechanism of oil adsorption in porous fibers.

Experimental Section

The electrospinning of fluorescent porous fibers

AIE-active PMMA powder with a molecular weight of 50,000 was dissolved in DMF with weight ratio of 30 wt%. The dissolved homogenous solutions were loaded into a 5 ml glass syringe connected with a metallic needle of 0.5 mm inner

diameter. The syringe was fixed horizontally onto a syringe pump (LSP02-1B, Baoding Longer Precision Pump Co., Ltd., China) with flow rate of 2 ml h^{-1}. A high voltage (10 Kv) was applied on the base of metallic needle and collector by a power supplier (DW-P303-1AC, Tianjin Dongwen High Voltage Co., China). A grounded copper plate used as a fiber collector was positioned at a distance of 150 mm from the tip of metallic needle. Temperature and humidity were controlled at 25 ℃ and 50 ± 5%, respectively.

Fabrication of PMMA porous/solid film

The porous film was prepared by spin-coating (WS-400-6NPp, Laurell Technologies Corporation, USA) at 3,000 rpm for 1 min. The solid film was produced by casting the solution on slide and drying at room temperature for 3 hours.

Characterization

Morphologies of surface and cross-section of porous/solid fiber and film were observed by a field emission scanning electron microscope (S-4800, Hitachi). Three-dimensional fluorescent image of PMMA fibrous membrane was captured by laser scanning confocal microscope (FV1000, Olympus). The optical and fluorescent microscope images of single PMMA porous fiber before and after oil adsorption were taken using an upright fluorescence microscope (BX51W1, Olympus). Fluorescence spectrum was carried out using a fluorescence spectrometer (FLS920, Edinburgh). The FLIM characterizations were carried out using a home-built optical system based on a Nikon optical microscope (Eclipse Ti) equipped with a motorized X-Y scanning stage and a time-correlated single photon counting module (PicoHarp 300, PicoQuant) coupled with an avalanche photodiode.

Results and Discussion

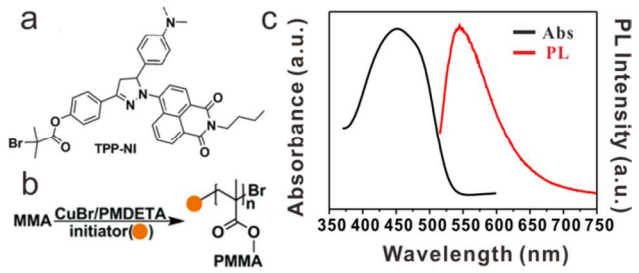

Figure. 1 (a) Formula of TPP-NI. (b) Scheme of a synthetic rout to polymer. (c) Absorption and emission spectra of the AIT-active PMMA.

Firstly, we synthesized an intramolecular charge transfer (ICT) and an AIE dual active initiator, TPP-NI based on our previously reported methods.[23] This molecule (**Figure 1**a) originated from a pyrazoline chromophore; it possesses an electron donor (dimethylamino), and an electron acceptor (l,8-naphthalimide). When TPP-NI was used as an ATRP initiator, the regular monomer methyl methacrylate (MMA) could be polymerized under moderate conditions as shown in **Figure 1**b. The absorption and emission spectra of the obtained α-end functionalized PMMA was shown in **Figure 1**c.

Then, following preparation, the AIE-active PMMA powder with a molecular weight of 50,000 was dissolved in N, N-Dimethylformamide (DMF) with weight ratio of 30 wt%. The solution was subsequently loaded into a 5 ml glass syringe and converted to fibers through the electrospinning method, as illustrated in **Figure 2**a. The mass-produced PMMA porous fibers were deposited on the collector to form a nonwoven yellow membrane, as shown in Figure S1. The average diameter of the

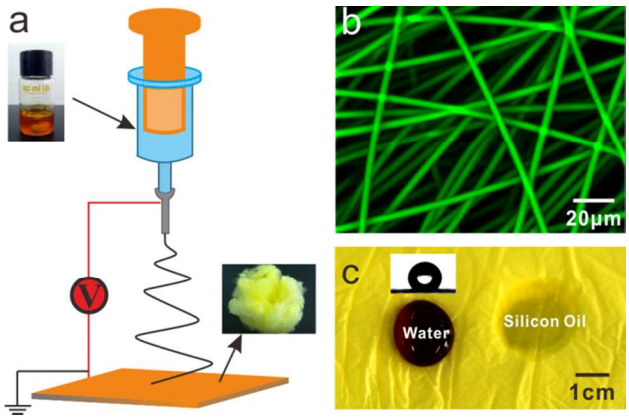

Figure. 2 (a) Schematic illustration of the electrospun fluorescent porous fibers. (b) Three-dimensional reconstruction of fluorescent PMMA porous fibers taken by laser confocal microscope. (c) The oleophilic and hydrophobic properties of the electrospun PMMA porous fibrous membrane. The water droplet was mixed with rhodamine B to make a distinction with the transparent silicon oil.

PMMA porous fibers is 4.2 ± 0.56 μm under certain electrospinning conditions (Figure S2), which emit significant yellow-green fluorescence with a 488 nm wavelength excitation. **Figure 2**b shows the fluorescent PMMA porous fibers under laser confocal microscope. The three-dimensional image reconstructed from the confocal scans reveals that the fluorescent fibers are arranged in a disordered fashion (Figure S3). The fibrous membrane exhibited hydrophobicity with a contact angle of 135°, while the silicon oil immediately adsorbed, as shown in **Figure 2**c.

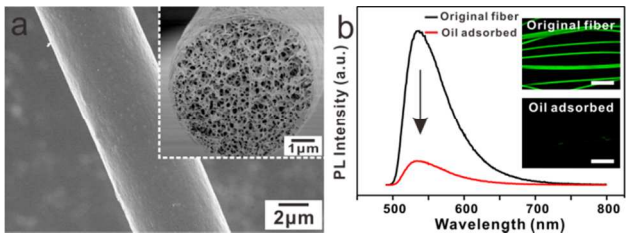

Figure. 3 (a) Surface and cross-sectional structures of PMMA porous fiber by SEM. (b) PL spectra of the PMMA porous fibers before and after silicon oil adsorption monitoring by the fluorescent microscope. The scale bar on the images is 50 μm.

The PMMA fiber was spun from the highly volatile DMF solution, which exhibited smooth surface and highly porous nanostructures, as shown in **Figure 3**a. It was noted that the photoluminescence (PL) intensity of the porous PMMA fibers dramatically decreased by a factor of 7.5 with oil adsorption. The images in **Figure 3**b, taken under microscope, show the fibers with fluorescent quenching.

The experiments were conducted to understand the mechanisms of fluorescent quenching in PMMA porous fibers after oil adsorption. The PMMA solid fibers were fabricated as shown in **Figure 4**a; the resultant fibers, electrospun from a highly volatile solvent (tetrahydrofuran (THF), boiling point of

66 ℃), had a smooth surface and solid core, as reported in literature.[25] More information on solid PMMA fibers can be found in the supplementary materials (Figure S4). The PL intensity of the solid fibers decreased by approximately 20% after the oil adsorption. **Figure 4**b depicts the change in fluorescence before and after oil adsorption, given equal exposure time.

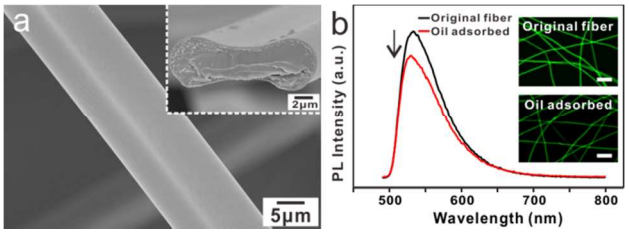

Figure. 4 (a) SEM micrograph of surface and cross section of PMMA solid fiber. (b) PL spectra of PMMA solid fibers before and after silicon oil adsorption, and the corresponding images under the fluorescent microscope. Scale bar is 100 μm.

It is clear that the structures of two fibers are entirely different. The specific surface area and porosity of the porous PMMA fibers are dramatically larger than the solid fibers. The measurements were done by nitrogen physical adsorption method, as shown in **Figure 5**a. According to the International Union and Applied Chemistry (IUPAC) classification,[25, 28] the adsorption-desorption isotherms of porous fiber can be categorized as type II with a distinct hysteresis loop characteristic of mesopores (2-50nm pore width) and macropores (>50nm). The porous fibers

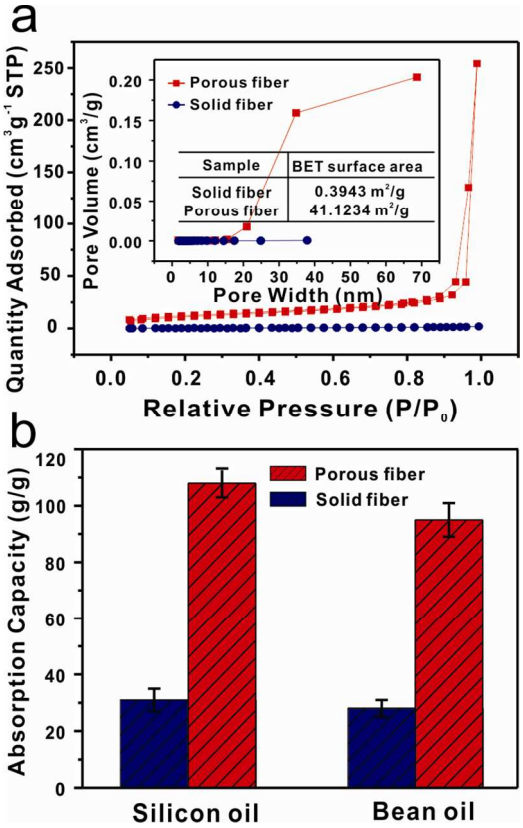

Figure. 5 (a) Nitrogen adsorption-desorption isotherms and pore size distribution curves of PMMA porous and solid fibers. (b) The adsorption capacities of PMMA porous and solid fibers for two different oils.

have a maximum nitrogen adsorption capacity of 254.33 $cm^3 g^{-1}$, which is approximately 141 times greater than that of the solid fibers (Figure S5). The porous fibers have a specific surface area of 41.1234 $m^2 g^{-1}$, approximately 100 times greater than the specific surface area of solid fibers (0.3943 $m^2 g^{-1}$). The pore size distributions of the fibers were measured by employing the Barrett–Joyner–Halenda (BJH) method, and clearly illustrate that porous fiber pore sizes are in the range of 15-70 nm. **Figure 5**b shows the oil adsorption capacity of two types of fibers, measured using silicon and bean oils. As expected, the porous fibers show much higher capacity for oil adsorption than solid fibers. The porous fibers' silicon and bean oil adsorption capacities are 108 and 95 g g^{-1} respectively. These adsorption capacity values are nearly three times higher than the capacity of the solid fibers. This ability is due to the porous fibers' ability to draw the oil into the interior pores of the fibers in addition to voids between the fibers.

Based on the above results, a possible model of the oil adsorption-induced fluorescence quenching mechanism displayed by PMMA porous fibers can be proposed. We hypothesize that the swelling of porous fibers changes the aggregation state of the AIE molecules, causing fluorescence quenching to occur due to the higher oil adsorption capacity of the porous fibers. **Figure 6**a shows a single PMMA porous fiber during oil adsorption, observed under an optical microscope. The superfluous silicon oil was dropped onto the fiber, and the size of the fiber was measured after 30 minutes. The original diameter of the fiber was approximately 4.32 μm, while the diameter of the fiber after oil adsorption increased to 5.58 μm, based on measurements from the microscopic images. Subsequently, the diameters of 50 different fibers were measured before and after oil adsorption, as shown in **Figure 6**a. The average diameter of the original fiber is 4.35 ± 0.27 μm, while after oil immersion, fibers swell to an average diameter of 5.43 ± 0.24 μm (enlargement of 20%). Simultaneously, the intensity of the bright field images dims due to the fluorescence quenching.

Figure 6b illustrates that the fluorescence quenching mechanism of porous fiber is due to the changes in the molecular aggregation state, which is disentangled as the swelling of the porous fibers after the oil adsorption. The intramolecular rotation behavior of AIE moiety (TPP-NI) anchored at the end of PMMA macromolecular chains was restricted by PMMA chains. The spatial constraint of the AIE molecules' rotation,restriction of intramolecular rotations (RIR),[29-31] is responsible for the AIE effect. The swelling of PMMA porous fibers caused by the penetration of oil molecules provides substantial space to allow for the unbinding of the intramolecular rotations of moieties. Under such circumstances, the photon energy absorbed by the AIE molecules is converted into kinetic energy (rotation and vibration) instead of being used to excite the electrons to a higher energy level.[32-33] This energy conversion causes the significant fluorescence quenching. Fluorescence lifetime imaging microscopy (FLIM) was used to monitor the fluorescence decays of PMMA porous fibers before and after oil adsorption. As shown in Figures S6a and b, the fluorescence intensity of PMMA porous fibers decreased dramatically after oil adsorption. The color change in the FLIM images (Figures S6c and d) implies a decrease in the fluorescence lifetime of PMMA porous fibers

after oil adsorption. The decay profiles shown in Figure S6e perfectly fit a tri-exponential function. A decrease of lifetime (by 2.00 ns) was observed with oil adsorption, consistent with the

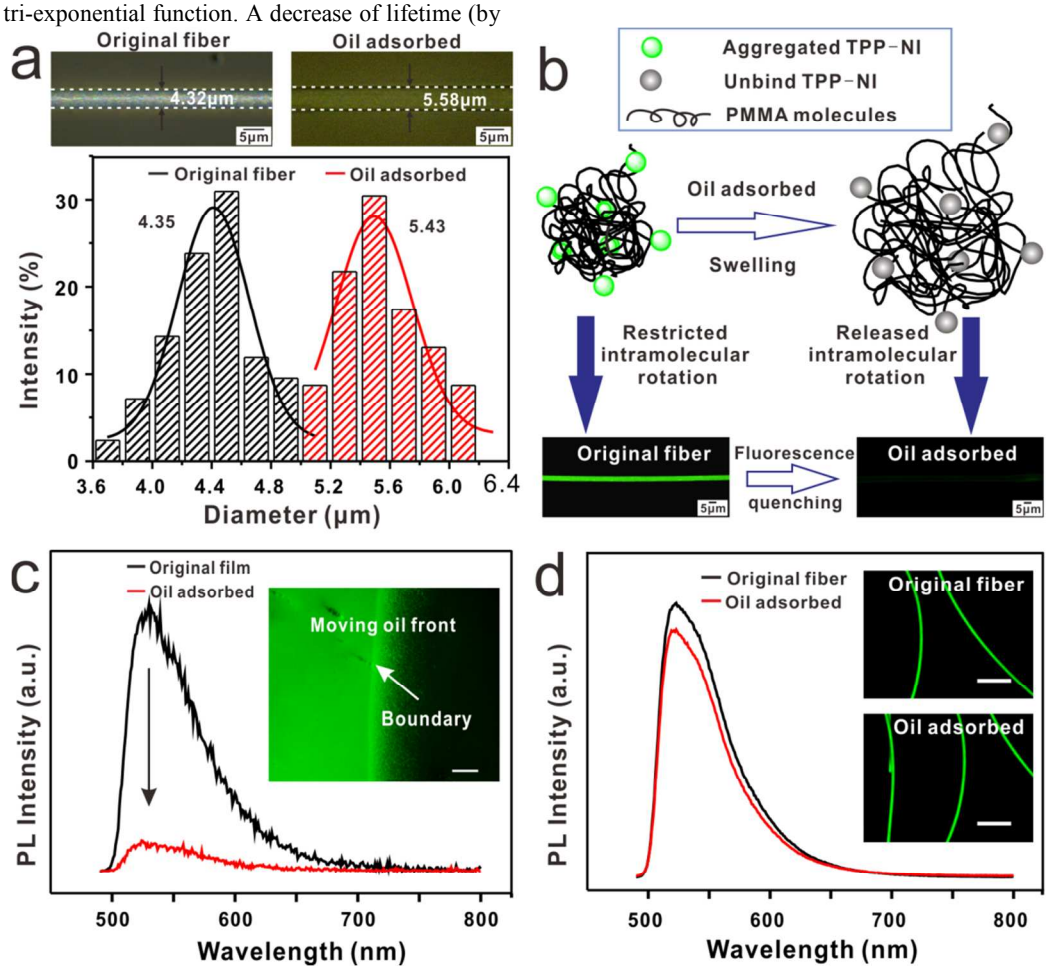

Figure. 6 (a) Size change of PMMA porous fibers before and after silicon oil adsorption. (b) Fluorescence quenching mechanism of the AIE-active porous fibers induced by oil adsorption. (c) PL spectra of PMMA porous film before and after silicon oil adsorption. Optical images of the moving boundary for oil adsorption under the fluorescent microscope. The scale bar is 100 μm. (d) PL spectra of PMMA/TPP-NI blend porous fibers before and after silicon oil adsorption and the corresponding images under the fluorescent microscope. The scale bars are 50 μm.

decrease in emission intensity compared with that of the PMMA porous fibers before oil adsorption (2.69 ns).

To further prove the above mechanism, we fabricated solid and porous films, shown in Figures S7a and S8, respectively. As expected, the oil is unable to permeate into the solid film, and its PL intensity and fluorescent image (Figure S7b) are unchanged before and after oil adsorption; the porous film has a similar fluorescence quenching behavior when immersed into oil. The PL intensity rapidly decreased by a factor of 8 after oil adsorption. It was noted that the front of the moving oil boundary can be clearly observed, strongly contrasting the fluorescent emission, as shown in the **Figure 6**c insert. These results reveal that with exposure to oil, the contacting surface area of the porous fiber and film is a critical factor in the quick swelling and fluorescence quenching effects observed after oil adsorption.

Pure PMMA solution was mixed with the fluorescent molecules (TPP-NI). The porous PMMA/TPP-NI composite fibers were electrospun; more information on this process can be found in the supplementary materials (Figure S9). As expected, the porous PMMA/TPP-NI composite fibers adsorb oil quickly, swelling. In contrast, the PL intensity of the porous PMMA/TPP-NI composite fibers decreased slightly and the corresponding fluorescent images were almost unchanged after the oil adsorption, as shown in **Figure 6**d. The distinct differences in the post-oil adsorption luminescence performances between the AIE-active PMMA porous fibers and PMMA/TPP-NI porous composite fibers further verifies the above-mentioned fluorescence quenching mechanism, revealing that the AIE-active PMMA porous fibers could be used as a material for oil sensors.

PMMA porous fibers have proven their capability for oil adsorption. However, the porous fibers should show repeated performance of good adsorption behaviour before it can be used for practical applications. **Figure 7**a shows the process of oil adsorption and desorption in PMMA porous fibers. 80 ml deionized water mixed with rhodamine B and 20 ml silicon oil were loaded in a 100 ml beaker. Following this step, 0.2 g

Cite this: DOI: 10.1039/c0xx00000x

www.rsc.org/xxxxxx

ARTICLE TYPE

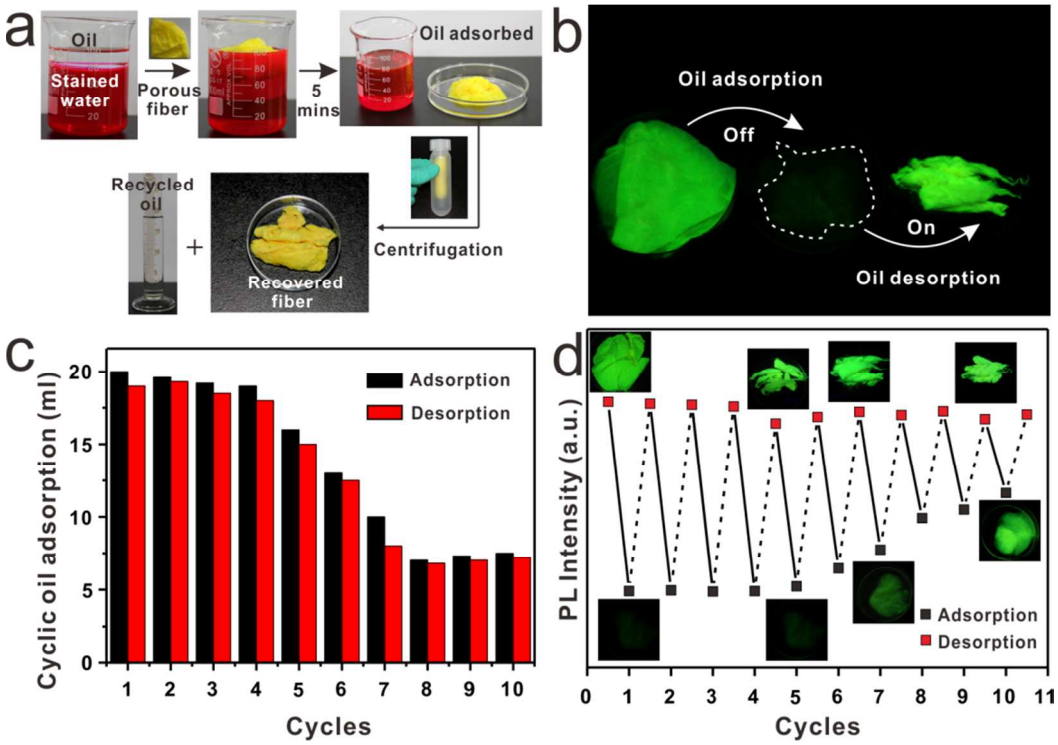

Figure. 7 (a) Process of the oil adsorption and desorption for PMMA porous fibers. (b) Switchable fluorescence (off/on) of PMMA porous fibers based on the process of oil adsorption and desorption. The fluorescent pictures were taken under 365 nm ultraviolet (UV) light, with a black background. (c) The capacity of oil adsorption and desorption of PMMA porous fibers with 10 cycles (d) PL intensity and corresponding fluorescent pictures of PMMA porous fibers with 10 cycles based on oil adsorption and desorption.

PMMA porous fibers in nonwoven fabric form were immersed into the mixture. The porous fibers adsorbed the oil quickly and swelled within a few minutes. To retain the porous structure of the fibers and extract the oil, the oil and fibers were subjected to centrifugation at a speed of 10,000 rpm (details in ESI, Figure S10). The volume of the recycled oil was 19 ml, as measured by a graduated flask. **Figure 7**c shows the cyclic silicon oil adsorption and desorption performance of PMMA porous fibers. For the first four cycles, the recovered volume was nearly the same as the adsorbed amount after each cycle. Although the fibers were squeezed by centrifugal force, the porous structures were undamaged, as shown in Figure S11. For each cycle up to the 4th cycle, the squeezed fibers swelled immediately after oil adsorption (Figure S12). However, after 5 cycles, the oil adsorption capacity of the porous fibers gradually decreased because the porous structure was destroyed by repeated centrifugation, as shown in Figure S13 (after 5 cycles) and Figure S14 (after 6 cycles). For each cycle after 7 cycles, the oil adsorption capacity of the porous fibers became almost unchanged, keeping a volume of approximately 7 ml (similar to the adsorption capacity of the solid fibers).

Figure 7b shows the switchable fluorescence of PMMA porous fibers based on the oil adsorption and desorption. The fluorescence of PMMA porous fibers can be tuned off by oil adsorption, as shown in **Figure 7**b. It is notable that after oil is desorbed from pores of PMMA fibers by centrifugation, the fluorescence can be tuned on. Observations made during the fluorescence quenching mechanism described previously (**Figure 6**b) indicate that the swelling PMMA fibers changed to the original state and restricted the intramolecular rotation of AIE moiety again, inducing the fluorescence to turn on. **Figure 7**d shows images and records of the cyclic PL intensity and fluorescence of PMMA porous fibers based on oil adsorption and desorption. The porous fibers showed three states during each cycle of oil adsorption and desorption: the initial state, the state after oil adsorption, and the state after oil desorption with centrifugation. The PL intensity of the non-woven PMMA porous fibers was initially extremely strong, and the fluorescence under UV light was bright yellow-green. The intensity decreased 7.5 times after oil adsorption and the fluorescence almost disappeared. The PL intensity of the PMMA porous fibers dramatically increased after oil desorption. Before completing 5 adsorption-desorption cycles, the switchable fluorescence (off/on) of PMMA porous fibers performed well each time. However, after 5 cycles, the PL intensity of the porous fibers after oil adsorption gradually increased, and the definition of the corresponding fluorescent pictures gradually improved. This effect was due to the damaged porous structure of the fibers as a

result of multiple centrifugation processes. The destroyed porous fibers behave like solid fibers. On the 10th adsorption-desorption cycle, the fluorescent picture of PMMA porous fibers was clearly captured, showing a bright yellow-green color. The reversible fluorescence of PMMA porous fibers shows that these fibers are promising for practical application as a material for oil adsorption sensors, as they are able to retain their porous structure.

Conclusions

In summary, AIE-active PMMA porous fibers with large specific surface areas were successfully prepared by using the electrospinning technique. The porous fibers exhibit excellent capability for oil adsorption. Due to fluorescence quenching induced by swelling, the PL intensity dramatically decreased after oil adsorption. The porous fibers' cyclic performance of oil adsorption may give rise to new perspectives concerning this study of material, and make it eligible for many practical applications. Furthermore, this study suggests that AIE-active polymers have a promising future in detection of oil adsorption. The present findings pave the way for future developments of sensitive AIE-active polymers detection by creating the porous structures.

Acknowledgement

We would like to thank Shuang Li and Prof. Qing-Hua Xu for their help with the fluorescence lifetime imaging microscopy (FLIM) measurements and Ya-Xin Zheng for her proofreading. We gratefully acknowledge the financial support from the National Science Foundation of China under Grants 51073113，91027039, 51373110 and 21071105 and the National Plan for Science and Technology Support (2012BAC14B03). We also acknowledge support from the Priority Academic Program Development of Jiangsu Higher Education Institutions (PAPD), Qing Lan Project for Excellent Scientific and Technological Innovation Team of Jiangsu Province (2012) and Project for Jiangsu Scientific and Technological Innovation Team (2013).

Notes and references

[a] *National Engineering Laboratory for Modern Silk; College for Textile and Clothing Engineering, Soochow University, Suzhou 215123, PR China; E-mail: kqzhang@suda.edu.cn*

[b] *College of Chemistry, Chemical Engineering and Materials Science; Key Laboratory of Absorption Technology for Wastewater Treatments in Petroleum and Chemical Industry, Soochow University, Suzhou 215123, PR China; Email: xuqingfeng@suda.edu.cn; lujm@suda.edu.cn*

† Electronic Supplementary Information (ESI) available: [massively-produced PMMA fibers, three-dimensional reconstructions of the fluorescent image of PMMA porous fibers, size distributions of porous and solid PMMA fibers, nitrogen adsorption-desorption isotherms and pore size distribution curves of PMMA solid fibers, fluorescence lifetime imaging microscopy analysis of PMMA porous fibers before and after oil adsorption, SEM images and PL spectra of PMMA solid film before and after oil immersion, SEM images of PMMA porous film, SEM images of PMMA/TPP-NI composite porous fiber, Detailed experimental procedures of oil recycle from PMMA porous fibers after oil adsorption by centrifugation.]. See DOI: 10.1039/b000000x/

1 D. Li, Y. Xia, *Adv. Mater.,* 2004, **16**, 1151.
2 A. Greiner, J. H. Wendorff, *Angew. Chem. Int. Ed.,* 2007, **46**, 5670.
3 W. Yuan, K.-Q. Zhang, *Langmuir*, 2012, **28**, 15418.
4 k. Friedemann, T. Corrales, M. Kappl, K. Landfester, D. Crespy, *Small*, 2012, **8**, 144.
5 C.-L. Zhang, K.-P. Lv, N.-Y. Hu, L. Yu, X.-F. Ren, S.-L. Liu, S.-H. Yu, *Small*, 2012, **8**, 2936.
6 F. Ko, Y. Gogotsi, A. Ali, N. Naguib, H. Ye, G. Yang, C. Li, P. Willis, *Adv. Mater.*, 2003, **15**, 1161.
7 S.Wang, Y. Zhang, H. Wang, G. Yin, Z. Dong, *Biomacromolecules*, 2009, **10**, 2240.
8 J. H. Yu, S. V. Fridrikh, G. C. Rutledge, *Adv. Mater.*, 2004, **16**, 1562.
9 A. Camposeo, L. Persano, D. Pisignano, *Macromol. Mater. Eng.*, 2013, **298**, 487.
10 J.-H. Syu, Y.-K. Cheng, W.-Y. Hong, H.-P. Wang, Y.-C. Lin, H.-F. Meng, H.-W. Zan, S.-F. Horng, G.-F. Chang, C.-H. Hung, Y.-C. Chiu, W.-C. Chen, M.-J. Tsai, H. Cheng, *Adv. Funct. Mater.*, 2012, **23**, 1566.
11 Y. Wang, A. La, Y. Ding, Y. Liu, Y. Lei, *Adv. Funct. Mater.*, 2012, **22**, 3547.
12 S. Yang, C.-F. Wang, S. Chen, *Angew. Chem. Int. Ed.*, 2011, **50**, 3706.
13 H.-J. Yen, C.-J. Chen, G.-S. Liou, *Chem. Commun.*, 2013, **49**, 630.
14 F. D. Benedetto, A. Camposeo, S. Pagliara, E. Mele, L. Persano, R. Stabile, R. Cingolani, D. Pisignano, *Nat. Nanotechnol.*, 2008, **3**, 614.
15 A. Camposeo, F. D. Benedetto, R. Stabile, A. A. R. Neves, R. Cingolani, D. Pisignano, *Small*, 2009, **5**, 562.
16 A. Camposeo, F. D. Benedetto, R. Stabile, R. Cingolani, D. Pisignano, *Appl. Phys. Lett.*, 2007, **90**, 143115.
17 X. Lu, Y. Zhao, C. Wang, *Adv. Mater.*, 2005, **17**, 2485.
18 X. He, L. Tan, X. Wu, C. Yan, D. Chen, X. Meng, F. Tang, *J. Mater. Chem.*, 2012, **22**, 18471.
19 H. Liu, J. B. Edel, L. M. Bellan, H. G. Craighead, *Small*, 2006, **2**, 495.
20 L. Persano, A. Camposeo, F. D. Benedetto, R. Stabile, A. M. Laera, E. Piscopiello, L. Tapfer, D. Pisignano, *Adv. Mater.*, 2012, **24**, 5320.
21 Y. Hong, J. W. Y. Lam, B. Z. Tang, *Chem. Commun.*, 2009, **29**, 4332.
22 Y. Hong, J. W. Y. Lam, B. Z. Tang, *Chem. Soc. Rev.*, 2011, **40**, 5361.
23 P.-Y. Gu, C.-J. Lu, F.-L. Ye, J.-F. Ge, Q.-F. Xu, Z.-J. Hu, N.-J. Li, J.-M. Lu, *Chem. Commun.*, 2012, **48**, 10234.
24 P. Dayal, J. Liu, S. Kumar, T. Kyu, *Macromolecules*, 2007, **40**, 7689.
25 J. Lin, B. Ding, J. Yang, J. Yu, G. Sun, *Nanoscale*, 2012, **4**, 176.
26 J. Lin, F. Tian, Y. Shang, F. Wang, B. Ding, J. Yu, *Nanoscale*, 2012, **4**, 5316.
27 J. Wu, N.Wang, L. Wang, H. Dong, Y. Zhao, L. Jiang, *ACS Appl. Mater. Interfaces*, 2012, **4**, 3207.
28 Kim, C.; Jeong, Y. I.; Ngoc, B. T. N.; Yang, K. S.; Kojima, M.; Kim, Y. A.; Endo, M.; Lee, J. W. *Small* **2007**, *3*, 91.
29 J. Chen, C. C. W. Law, J. W. Y. Lam, Y. Dong, S. M. F. Lo, I. D. Williams, D. Zhu, B. Z. Tang, *Chem. Mater.*, 2003, **15**, 1535.
30 X. Fan, J. Sun, F. Wang, Z. Chu, P. Wang, Y. Dong, R. Hu, B. Z. Tang, D. Zou, *Chem. Commun.*, 2008, **26**, 2989.
31 E. P. J. Parrott, N. Y. Tan, R. Hu, J. A. Zeitler, B. Z. Tang, E. P. MacPherson, *Mater. Horiz.*, DOI**:** 10.1039/C3MH00078H.
32 K. S. Wong, H. Wang, G. Lanzani, *Chem. Phys. Lett.*, 1998, **288**, 59.
33 J. W. Barr, T. W. Bell, V. J. Catalano, J. I. Cline, D. J. Phillips, R. Procupez, *J. Phys. Chem. A*, 2005, **109**, 11650.